Eur. Phys. J. Plus (2022) 137:1197
https://doi.org/10.1140/epjp/s13360-022-03332-z

THE EUROPEAN PHYSICAL JOURNAL PLUS

Investigation of analog resistive switching in ZrO_2 nanostructured film

Aman Sharma[1], **Mohd Faraz**[2], **Neeraj Khare**[1,2,a]

[1] Department of Physics, Indian Institute of Technology Delhi, Hauz Khas, New Delhi 110016, India
[2] Nanoscale Research Facility (NRF), Indian Institute of Technology Delhi, Hauz Khas, New Delhi 110016, India

Received: 8 July 2022 / Accepted: 27 September 2022
© The Author(s), under exclusive licence to Società Italiana di Fisica and Springer-Verlag GmbH Germany, part of Springer Nature 2022

Abstract In this article, we report the synthesis of Zirconium Oxide (ZrO_2) nanostructure by hydrothermal method and fabrication of resistive switching device [FTO/ZrO_2/Ag] using spray coated ZrO_2 nanostructured film. The XRD spectrum of the film indicates the formation of a single-phase ZrO_2 nanostructure. I–V measurement of the fabricated device shows gradual set and reset at 0.8 and − 0.7 V, respectively, which confirms the presence of analog switching in the device. The conduction mechanism has been explored with a I–V fitting model in high resistive state and low resistive state, respectively. In high resistive state, the device stays in the ohmic region at lower bias however at higher bias due to filling of available traps the electrical transport is dominated by space charge limited conduction (SCLC). On the other hand, in low resistive state, charge carriers are detrapped and the electrical conduction process is again governed by SCLC conduction.

1 Introduction

The increasing demand for data storage and computing applications has attracted researchers toward resistive random-access memory (ReRAM) devices due to its low power consumption, high operating speed, reduced potential, and compatibility with complementary metal-oxide-semiconductor (CMOS) technology [1, 2]. The ReRAM is a simple capacitor device that consists of an insulating/semiconducting layer sandwiched between two metal electrodes. The ReRAM device is capable of switching between two or more resistance states upon applying a bias voltage [3, 4]. ReRAM devices have been fabricated using different metal oxides such as tungsten oxide [5], tantalum oxide [6], nickel oxide [7], titanium oxide [8], hafnium oxide [9], zinc oxide [10], and cobalt ferrite [11]. Oxide based ReRAM devices have been mostly observed to exhibit digital switching. However, there are few reports of the observation of analog switching also [12–17]. The electroforming free resistive switching can also be realized using nanostructured material [18].

ReRAM device can be used as synaptic device for neuromorphic computing but for these application ReRAM devices must exhibit analog switching [14, 15]. Recently there are reports on observing analog switching in inorganic oxide materials like titanium oxide [15], zinc oxide [16], and tantalum oxide [17]. Among all the oxide materials, ZrO_2 can also be interesting material to explore resistive switching as it has high dielectric constant, large bandgap, stable thermal properties and can exhibit resistive switching at low bias field [19]. ZrO_2 films are prepared via sol–gel deposition technique, sputtering technique, and atomic layer deposition technique [4, 19, 20]. Lee et al. studied the effect of UV irradiation on the switching properties of ZrO_2 films which showed stable digital resistive switching property after UV irradiation [21]. Lee et al. reported the presence of synaptic characteristics after insertion of SiO_2 thin films in Cu/SiO_2/ZrO_2/Pt devices [22].

In the present work, we report the synthesis of ZrO_2 nanorods by hydrothermal method and the fabrication of FTO/ZrO_2/Ag resistive switching device using ZrO_2 nanostructured film exhibiting analog switching. The mechanism of resistive switching is also presented by analyzing I–V characteristics of the device in high resistive and low resistive state.

2 Experimental details

2.1 Material synthesis

The ZrO_2 nanostructured powder was prepared using the hydrothermal method [23]. Initially, 0.5 M zirconyl nitrate hydrate ($ZrO(NO_3)_2.xH_2O$) solution was prepared in deionized (DI) water. 5 M NaOH solution prepared in DI water was slowly added to

[a] e-mail: nkhare@physics.iitd.ernet.in (corresponding author)

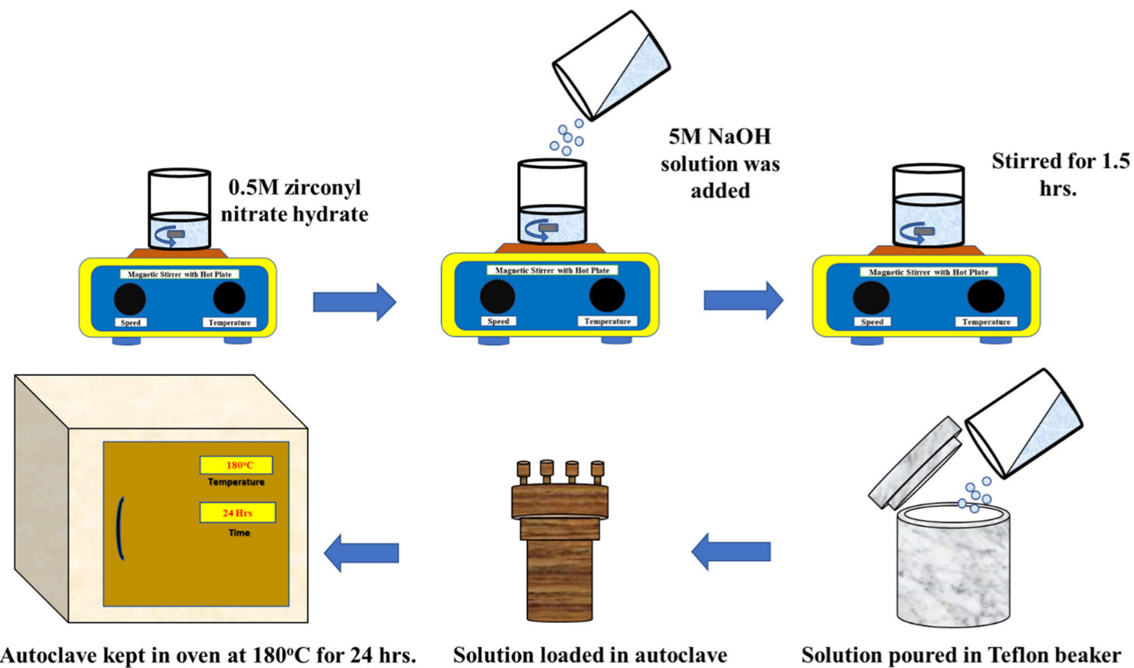

Fig. 1 Schematic for synthesis of ZrO_2 powder

Fig. 2 Schematic of FTO/ZrO_2/Ag resistive switching device

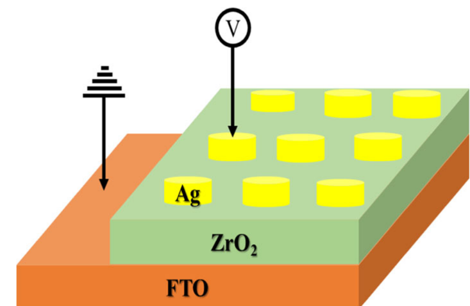

zirconyl nitrate solution under continuous stirring followed by sonication for 30 min to obtain a homogeneous solution. A 70 ml of the prepared solution was loaded into a 100 ml Teflon-lined autoclave.

The autoclave was sealed and maintained at temperature 180 °C for 24 h (hydrothermal treatment time). It was then allowed to cool down to room temperature naturally. The resultant precipitate was filtered, washed with distilled water to remove the soluble nitrates, and with ethanol to reduce agglomeration, and later dried at 100 °C for 12 h. This ZrO_2 powder was used as the precursor for the fabrication of ZrO_2 thin film on the FTO substrate using spray deposition technique (Fig. 1).

2.2 Device fabrication

The FTO/ZrO_2/Ag trilayer structure (Fig. 2) was fabricated using ZrO_2 film which was deposited by spray coating the ZrO_2 nanopowder on the FTO substrate. Before deposition of the film, the FTO substrate was cleaned via the conventional ultrasonication method (ultrasonication in deionized water, acetone, and isopropyl alcohol for 10 min each). A part of the FTO substrate was covered with Kapton tape for getting the bottom contact of the device. ZrO_2 powder was mixed in ethanol and was stirred for 30 min. Afterward, a diluted citric acid (in DI water) was slowly added to ZrO_2. The resultant solution was loaded in a spray gun and was spray coated precisely on the FTO substrate. The thickness of the ZrO_2 film was 350 nm. After the deposition, the film was dried at 80 °C for an hour. The contact pads of Silver (Ag) on the device were deposited by e-beam evaporator using metal shadow mask with holes of diameter 0.5 mm. The thickness of the silver contact pad on ZrO_2 film was 100 nm.

2.3 Characterizations

In order to characterize the ZrO_2 film grown on FTO substrate, powder X-ray diffraction (XRD) was performed on a Rigaku Ultima IV diffractometer equipped with Ni-filtered Cu Kα radiation (1.54 Å) [24]. Diffraction patterns were recorded for this film in the

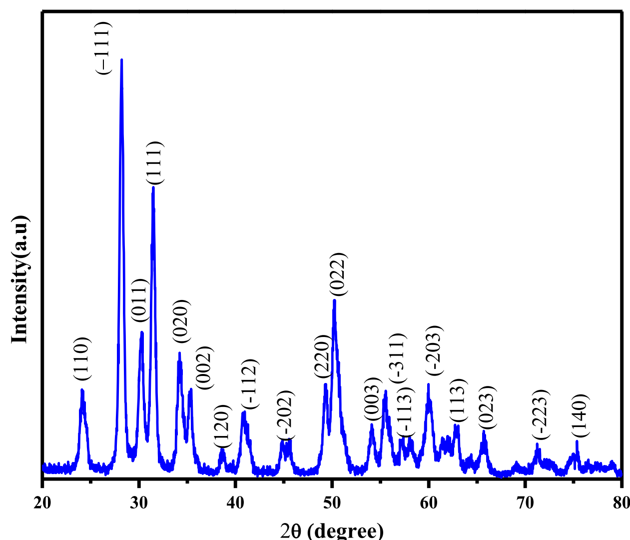

Fig. 3 XRD pattern of ZrO_2 nanostructured film spray deposited on FTO substrate

range of 2θ from 20° to 80° at a scanning rate of 2°/min. A scanning electron microscope (SEM, TM3000, Hitachi) equipped with an EDAX (SwiftED3000 Oxford) was used to collect SEM images and to analyze composition [25]. FEI Tecnai transmission electron microscope (accelerating voltage = 200 kV) was used to conduct a transmission electron micrograph (TEM) [26]. Electrical transport measurement was performed by Keithley 2400 source meter. Two probe point contact was made on the device with a sharp conducting probe tip made of copper. The data of current (I) versus voltage (V) were recorded via Labview interfaced computer program.

3 Result and discussion

X-ray diffractometer (XRD) pattern of ZrO_2 nanorods is shown in Fig. 3. The XRD pattern of ZrO_2 nanorods has the characteristic peaks at 24.20°, 28.40°, 30.46°, 31.71°, 34.12°, 35.52°, 38.57°, 40.87°, 44.67°, 49.38° and 50.15° corresponding to (110), (− 111), (011), (111), (020), (002), (120), (− 112), (− 202), (220) and (022) planes, respectively (JCPDS card no. 37–1484). No unidentified peaks were observed in the XRD pattern, indicating the synthesis of single-phase ZrO_2. The average crystallite size of ZrO_2 nanorods was obtained as ∼ 50 nm. Scherer formula is used to determine the average crystallite size for ZrO_2 nanorods, which is given as [27];

$$t = \frac{0.9\lambda}{\beta \cos\theta} \tag{1}$$

where β represents the full width at half the maximum of the XRD peak, θ is Bragg's angle, (1.542 Å) is the wavelength of X-ray, and t is the average crystallite size. The average crystallite sizes for ZrO_2 nanorods are estimated as ~ 50 nm, respectively.

The morphology and chemical composition of the ZrO_2 nanostructure were studied by SEM and EDAX analysis. The SEM image of the ZrO_2 nanostructure is shown in Fig. 4a. The ZrO_2 nanostructure shows the irregular-shaped overlapped morphology due to the aggregation of nanorods. The chemical composition of the ZrO_2 nanorods was examined by EDAX (Fig. 4b) which shows that the Zr and O elements are present in the stoichiometric ratio.

The TEM micrograph of ZrO_2 nanostructure was recorded to determine the shape, size, and uniformity of the nanorods. The TEM micrograph of ZrO_2 nanostructure shows the nanorods-like structure (Fig. 4c) with the average length of the nanorods as 45 nm, as observed by the size distribution histograms (Fig. 4 d).

4 Electrical transport properties

For recording of I–V characteristics of the device a direct current (DC) voltage sweep from 0 → 1 → 0 → − 1 → 0 with a step of 0.01Volt and a maximum applied voltage of 1 V with compliance current (I_{CC}) of 10 mA was applied and the result is shown in Fig. 5a. In the first voltage sweep 1, the device was in the high-resistance state (HRS). In the resistive cycle, on returning from 1 → 0 there is a gradual change in the resistance, and the device switches from HRS (high-resistance state) to LRS (low-resistance state) at 0.8 Volt. Similarly, in cycle 3(0 → − 1) device stays in the LRS state, and the cycle from − 1 → 0 around—0.7 V the device switches to HRS again. I–V characteristics of the $FTO/ZrO_2/Ag$ device were recorded for several cycles to check the reproducibility of switching device. Figure 5b shows the I–V characteristics for 1 to 100th cycle at each 10th interval. Exact overlapping of all I–V

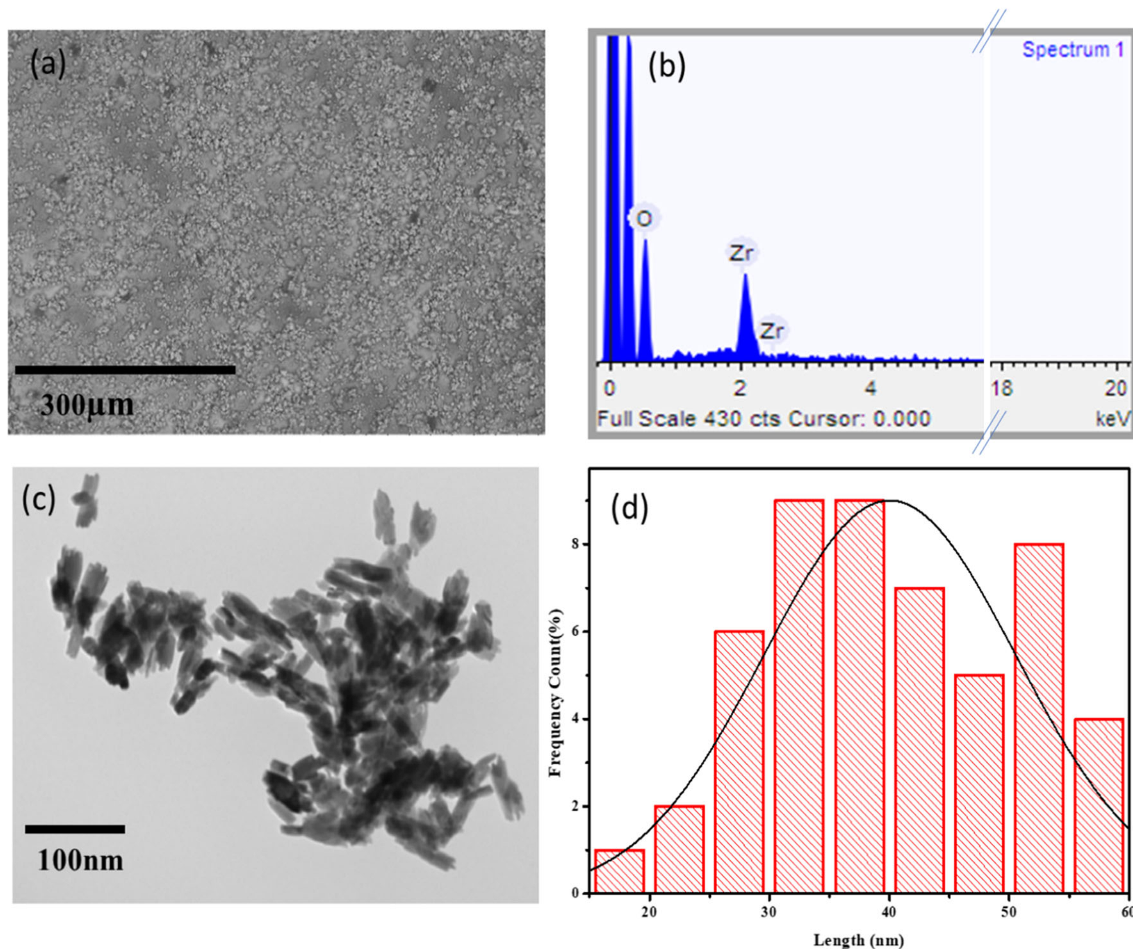

Fig. 4 **a** SEM image and, **b** EDAX patterns of ZrO_2 nanorods, **c** TEM images of ZrO_2 nanorods and **d** Size distribution histograms of ZrO_2 nanorods

characteristics clearly shows that the performance of resistive switching is very stable. A small switching window can be seen in all the cycles. As in all 100 cycles, there is a small change in the resistance between the HRS and LRS, and there is no sharp transition between the HRS and LRS, the switching of device can be described as analog switching. Figure 5c shows the resistance values in both LRS and HRS with $R_{\text{off}}/R_{\text{on}}$ ratio as 1.86 at 0.35Volt. The I–V measurement was performed on 6 devices and we got similar kind of switching pattern as show in Fig. 5c. We have also performed the experiment for − 2 to + 2 Volt separately and it has been observed for 2 Volt of applied bias, the device shows breakdown behavior and no switching window is seen Similar type of behavior of occurring breakdown for higher applied bias is reported in earlier also [28].

5 Mechanism of switching

In the present device, the HRS to LRS switching is not abrupt and there is a continuous variation for changing for HRS to LRS. In order to understand the mechanism of the present analog switching, we carried out a detailed analysis of I–V characteristics both in HRS and LRS. In Fig. 6a, b, I–V characteristics have been plotted in logarithmic scale for both HRS and LRS. It is observed that the initial bias voltage the variation of current (I) with voltage (V) is linear however for larger bias the characteristics become nonlinear. For the HRS, the slope of the ln-I-ln-V curve is 2 for the bias voltage from $V_1 = 0.23$ Volts to $V_2 = 0.53$ Volts, and for $V > 0.53$ Volts the slope becomes 3. For LRS, the slope of I–V is equal to 2 from 1 to 0.25 Volts, and it is equal to 1 from 0.25 to 0 Volts of applied bias.

The ohmic conduction equation is given by [29]

$$J_{\text{ohmic}} = \sigma E = q\mu N_c E \exp\left[\frac{-(E_{\text{c}} - E_{\text{F}})}{KT}\right] \tag{2}$$

where σ is electrical conductivity, μ is the electron mobility, Nc is the effective density of states of the conduction band, EC is the conduction band and EF is the Fermi energy level. The current (I)–Voltage (V) characteristics of the present resistive switching

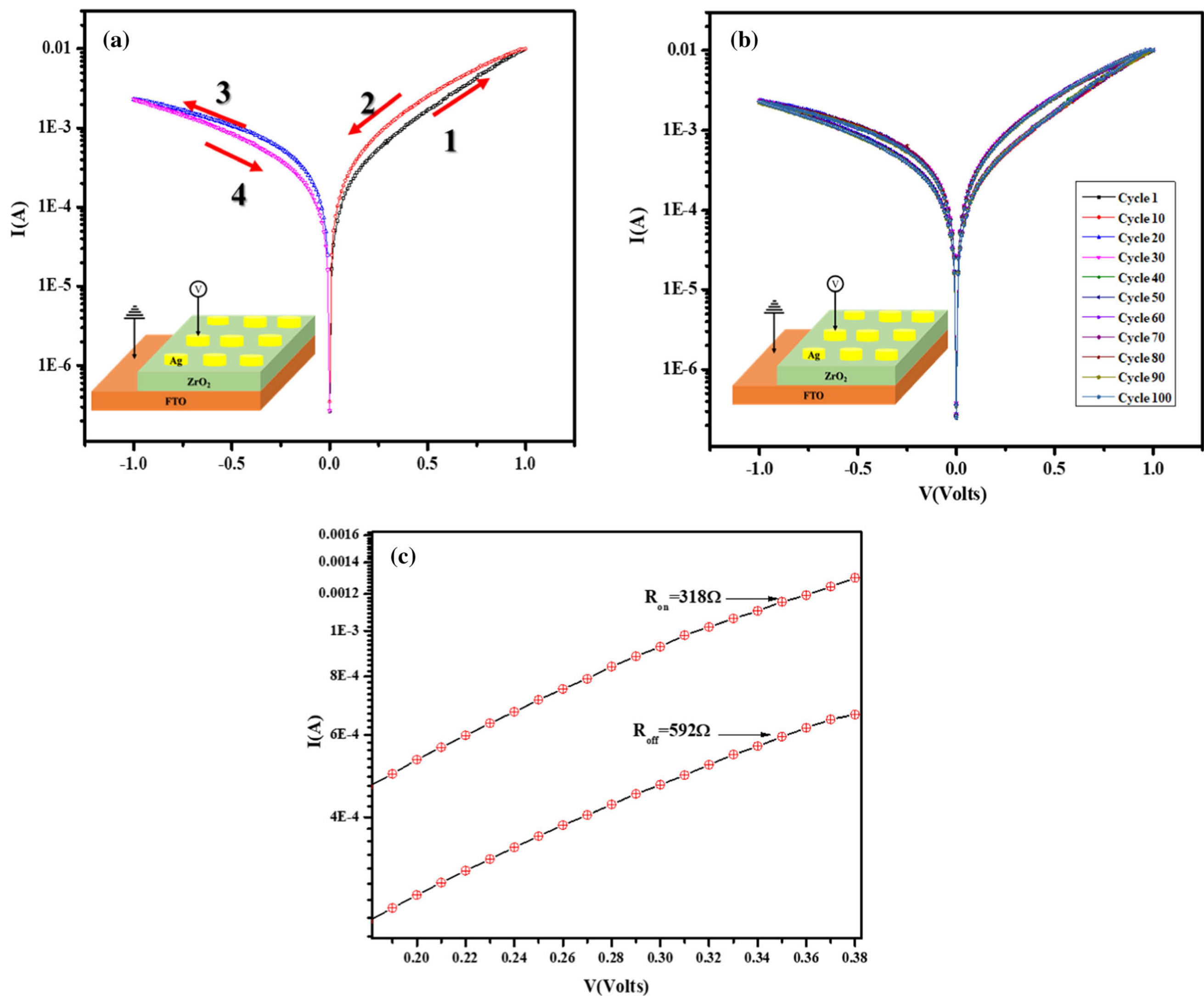

Fig. 5 **a** I–V measurement of FTO/ZrO_2/Ag device with $V_{\max} = \pm 1$Volt, (**b**). Repeated cycles of I–V characteristics from 1to 100th cycles, (**c**). Magnified view of resistance values in on and off state of device

device follows $I\ \alpha$ Vm [30, 31] which is a clear signature that the trap assisted space charge limited conduction (SCLC) is the dominant mechanism of charge traps.

Conduction process in our device is influenced by trapping and de-trapping of charge carriers in an externally applied electric field. In the trapping/de-trapping mechanism of conduction, the trapping of charges provides a conduction path and thus increases the current [31, 32]. For the cycle $0 \rightarrow 1$, when biasing voltage is less than 0.23 Volt thermally generated charge carriers dominate and the ohmic conduction takes place for which the slope (m) is equal to 1. When the biasing voltage is raised from 0.23 Volt to 053 Volt the traps (voids/defect) states got occupied by the charge carriers. As the traps getting filled, it becomes easier for electrons to flows and there is a rise in current which leads the slope (m) equals to 2 [31, 32]. Further increasing the applied bias voltage ($0.53 < V < 1$), all the traps present in the film got filled with the charge carriers and the current is increased further which changes the slope (m) from 2 to 3. In the phenomenon of trapping, more number of charges present in the active layer which form a conduction path between top and bottom electrode. The process of conduction happens due to trap assisted space charge limited conduction (TSCLC) in the active layer this leads the exponential rise in the current [31]. For the cycle $1 \rightarrow 0$, initially, trap states were filled with the charges. As the applied voltage is decreased from 1 to 0 Volt, the charges start de-trapping from its trapping centers due to presence of opposite lower applied bias. Although the de-trapping of charges got started, there are still trapped charges till 0.25 Volt which causes the slope (m) equals to 2. Due to few trapped charges in the film till 0.25 volts the conduction process is again governed by the TSCLC process. Further when the charges got fully de-trapped below 0.25 Volt, the ohmic conduction process is dominated which causes the slope (m) to change from 2 to 1 [31–33].

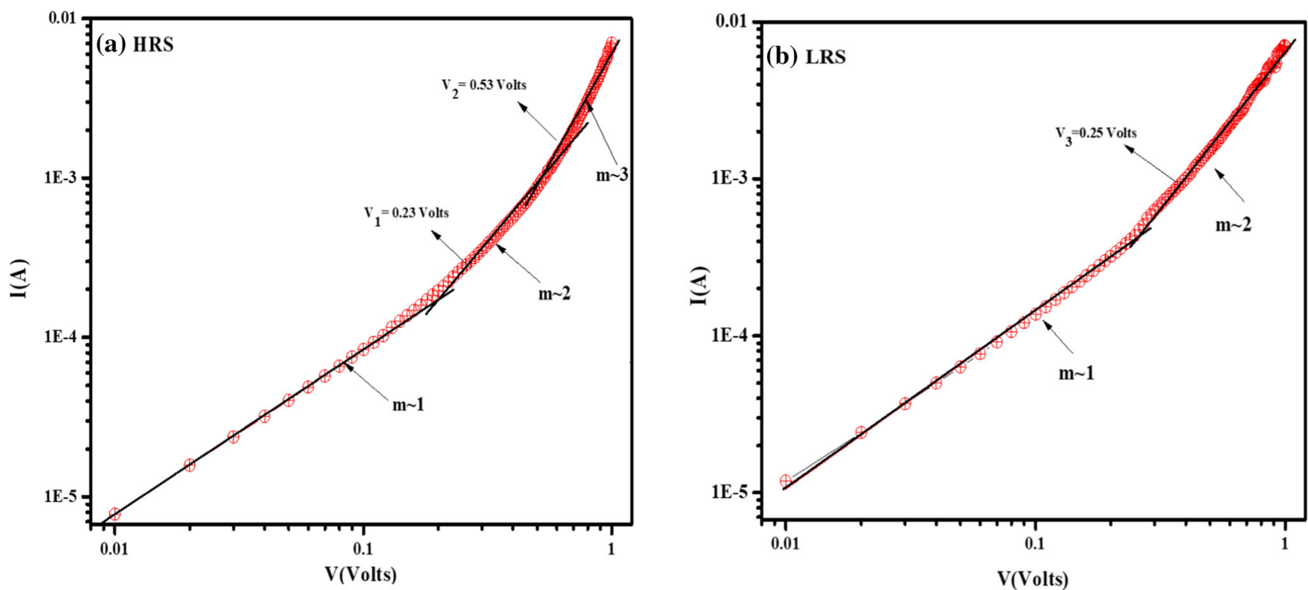

Fig. 6 Experimental I–V curve fitted to $I = KV^m$ for the resistive switching devices, **a** High Resistance State (HRS), and **b** Low Resistance State (LRS)

6 Conclusions

Analog resistive switching device with FTO/ZrO_2/Ag structure was fabricated using spray deposited ZrO_2 nanostructured film. ZrO_2 nanostructure was prepared using the hydrothermal technique. XRD studies confirmed the formation of single-phase ZrO_2 film and the TEM micrograph of ZrO_2 nanorods showed the nano-rod-like structure. The fabricated device exhibits analog switching behavior with gradual switching from HRS to LRS with the resistance ratio R_{on}/R_{off} as 1.86 at 0.35 Volts. Analysis of I–V characteristics of HRS and LRS revealed that in the higher applied bias transport is dominated by SCLC mechanism and the switching for HRS to LRS is due to filling and unfilling of trap states.

Acknowledgements We are grateful for the financial support provided through NNetRA by the Ministry of Electronics and Information Technology (MeitY, project no. RP03530) and the Department of Science and Technology (DST, project no. MI01756). Nanoscale Research Facility (NRF) is highly acknowledged for using several characterization facilities. One of the authors, A. S. is grateful to IIT Delhi for providing the institute research fellowship.

Data Availability Statement No Data associated in the manuscript.

References

1. S. Munjal, N. Khare, Advances in resistive switching based memory devices. J. Phys. D Appl. Phys. **52**, 433002 (2019)
2. C.-H. Lai, C.-Y. Liu, H. Yang, Bipolar resistance switching characteristics in zirconium oxide. Ferroelectrics **457**, 146–152 (2013)
3. H. Mähne, H. Wylezich, F. Hanzig, S. Slesazeck, D. Rafaja, T. Mikolajick, Analog resistive switching behavior of Al/Nb_2O_5/Al device. Semicond. Sci. Technol. **29**, 104002 (2014)
4. Y. Yuan, X. Cao, Y. Sun, J. Su, C. Liu, L. Cheng, Y. Li, L. Yuan, H. Zhang, J. Li, Intrinsic mechanism in nonvolatile polycrystalline zirconium oxide sandwiched structure. J. Mater. Sci. Mater. Electron. **29**, 2301–2306 (2018)
5. W. Chien, Y. Chen, E. Lai, F. Lee, Y. Lin, A.T. Chuang, K. Chang, Y. Yao, T. Chou, H. Lin, A study of the switching mechanism and electrode material of fully CMOS compatible tungsten oxide ReRAM. Appl. Phys. A **102**, 901–907 (2011)
6. Y. Ma, D. Li, A.A. Herzing, D.A. Cullen, B.T. Sneed, K.L. More, N. Nuhfer, J.A. Bain, M. Skowronski, Formation of the conducting filament in TaO_x-resistive switching devices by thermal-gradient-induced cation accumulation. ACS Appl. Mater. Interfaces **10**, 23187–23197 (2018)
7. M. Chowdhury, B. Long, R. Jha, V. Devabhaktuni, A fundamental understanding of nickel oxide based resistive random access memory with high percentage of oxygen. Solid State Electron. **68**, 1–3 (2012)
8. A. Kumari, S.M. Shanbogh, I. Udachyan, S. Kandaiah, A. Roy, V. Varade, A. Ponnam, Interface-driven multifunctionality in two-dimensional TiO_2 nanosheet/poly (dimercaptothiadiazole-triazine) hybrid resistive random access memory device. ACS Appl. Mater. Interfaces **12**, 56568–56578 (2020)
9. S. Yu, R. Jeyasingh, Y. Wu, H.-S.P. Wong, Characterization of low-frequency noise in the resistive switching of transition metal oxide HfO_2. Phys. Rev. B **85**, 045324 (2012)
10. D. Khakhulin, Z. Vakulov, V. Smirnov, R. Tominov, J.-G. Yoon, O. Ageev, Resistive switching in ZnO/ZnO: in nanocomposite, in: *Journal of Physics: Conference Series*, IOP Publishing, (2017), pp. 092008
11. S. Munjal, N. Khare, Multilevel resistive and magnetization switching in Cu/$CoFe_2O_4$/Pt device: coexistence of ionic and metallic conducting filaments. Appl. Phys. Lett. **113**, 243501 (2018)
12. T.D. Dongale, A.C. Khot, A.V. Takaloo, K.R. Son, T.G. Kim, Multilevel resistive switching and synaptic plasticity of nanoparticulated cobaltite oxide memristive device. J. Mater. Sci. Technol. **78**, 81–91 (2021)

13. X. Li, H. Wu, B. Gao, W. Wu, D. Wu, N. Deng, J. Cai, H. Qian, Electrode-induced digital-to-analog resistive switching in TaO_x-based RRAM devices. Nanotechnology **27**, 305201 (2016)
14. F. Cüppers, S. Menzel, C. Bengel, A. Hardtdegen, M. Von Witzleben, U. Böttger, R. Waser, S. Hoffmann-Eifert, Exploiting the switching dynamics of HfO_2-based ReRAM devices for reliable analog memristive behavior. APL Mater. **7**, 091105 (2019)
15. Y.-F. Wang, Y.-C. Lin, I. Wang, T.-P. Lin, T.-H. Hou, Characterization and modeling of nonfilamentary $Ta/TaO_x/TiO_2/Ti$ analog synaptic device. Sci. Rep. **5**, 1–9 (2015)
16. F.M. Simanjuntak, T. Ohno, S. Chandrasekaran, T.-Y. Tseng, S. Samukawa, Neutral oxygen irradiation enhanced forming-less ZnO-based transparent analog memristor devices for neuromorphic computing applications. Nanotechnology **31**, 26LT01 (2020)
17. W.-J. Chen, C.-H. Cheng, P.-E. Lin, Y.-T. Tseng, T.-C. Chang, J.-S. Chen, Analog resistive switching and synaptic functions in WO_x/TaO_x bilayer through redox-induced trap-controlled conduction. ACS Appl. Electron. Mater. **1**, 2422–2430 (2019)
18. S. Munjal, N. Khare, Electroforming free controlled bipolar resistive switching in $Al/CoFe_2O_4/FTO$ device with self-compliance effect. Appl. Phys. Lett. **112**, 073502 (2018)
19. S.-J. Park, B.-S. Yu, J.-Y. Jeon, B.-C. Kang, T.-J. Ha, Sol-gel based zirconium dioxide dielectrics by oxygen-annealing at low temperature for highly stable and robust flexible resistive random access memory. J. Alloy. Compd. **825**, 154086 (2020)
20. A.A. Sivkov, Y. Xing, Z. Minden, Z. Xiao, K.Y. Cheong, F. Zhao, Resistive switching properties of ZrO_2 film by plasma-enhanced atomic layer deposition for non-volatile memory applications. J. Electron. Mater. **50**, 5396–5401 (2021)
21. Y. Lee, J. Jung, D. Shin, J.J. Pak, Effect of UV irradiation on the resistive switching characteristics of low-temperature solution-processed ZrO_2 RRAM. Semicond. Sci. Technol. **36**, 085004 (2021)
22. D. Lee, A.S. Sokolov, B. Ku, Y.-R. Jeon, H.T. Kim, G.H. Kim, C. Choi, Improved switching and synapse characteristics using PEALD SiO_2 thin film in $Cu/SiO_2/ZrO_2/Pt$ device. Appl. Surf. Sci. **547**, 149140 (2021)
23. M.Z. Ansari, M. Faraz, S. Munjal, V. Kumar, N. Khare, Highly dispersible and uniform size Cu_2ZnSnS_4 nanoparticles for photocatalytic application. Adv. Powder Technol. **28**, 2402–2409 (2017)
24. W. Raza, M. Faraz, Novel g-C_3N_4/Fe-ZnO/RGO nanocomposites with boosting visible light photocatalytic activity for MB, Cr (VI), and outstanding catalytic activity toward para-nitrophenol reduction. Nanotechnology **31**, 325603 (2020)
25. S. Kumar, M. Faraz, N. Khare, Enhanced thermoelectric properties of Sb_2Te_3-graphene nanocomposite. Mater. Res. Express **6**, 085079 (2019)
26. M. Faraz, H.H. Singh, N. Khare, A progressive strategy for harvesting mechanical energy using flexible PVDF-rGO-MoS_2 nanocomposites film-based piezoelectric nanogenerator. J. Alloys Compd. **890**, 161840 (2022)
27. A.K. Gautam, M. Faraz, N. Khare, Enhanced thermoelectric properties of tungsten oxide-reduced graphene oxide nanocomposites. Ceram. Int. **47**, 27885–27889 (2021)
28. T.S. Bhat, C.C. Revadekar, S.S. Patil, T.D. Dongale, D.K. Kim, P.S. Patil, Photo-induced resistive switching in CdS-sensitized TiO_2 nanorod array memristive device. J. Mater. Sci. Mater. Electron. **31**(13), 10919–10929 (2020)
29. E.W. Lim, R. Ismail, Conduction mechanism of valence change resistive switching memory: a survey. Electronics **4**, 586–613 (2015)
30. D. Shang, Q. Wang, L. Chen, R. Dong, X. Li, W. Zhang, Effect of carrier trapping on the hysteretic current-voltage characteristics in Ag/ $La_{0.7}$ $Ca_{0.3}$ MnO_3/ Pt heterostructures. Phys. Rev. B **73**, 245427 (2006)
31. M.M. Rehman, B.S. Yang, Y.J. Yang, K.S. Karimov, K.H. Choi, Effect of device structure on the resistive switching characteristics of organic polymers fabricated through all printed technology. Curr. Appl. Phys. **17**(4), 533–540 (2017)
32. Y. Cui, H. Peng, S. Wu, R. Wang, T. Wu, Complementary charge trapping and ionic migration in resistive switching of rare-earth manganite $TbMnO_3$. ACS Appl. Mater. Interfaces **5**(4), 1213–1217 (2013)
33. T. You, N. Du, S. Slesazeck, T. Mikolajick, G. Li, D. Bürger, I. Skorupa, H. Stöcker, B. Abendroth, A. Beyer, K. Volz, Bipolar electric-field enhanced trapping and detrapping of mobile donors in $BiFeO_3$ memristors. ACS Appl. Mater. Interfaces **6**(22), 19758–19765 (2014)

Springer Nature or its licensor (e.g. a society or other partner) holds exclusive rights to this article under a publishing agreement with the author(s) or other rightsholder(s); author self-archiving of the accepted manuscript version of this article is solely governed by the terms of such publishing agreement and applicable law.